AD-A165 536 DIRECT NUMERICAL SIMULATION OF AXISYMMETRIC JETS(U) 1/1
NAVAL RESEARCH LAB WASHINGTON DC F F GRINSTEIN ET AL.
25 MAR 86 NRL-MR-5732

UNCLASSIFIED F/G 20/4 NL

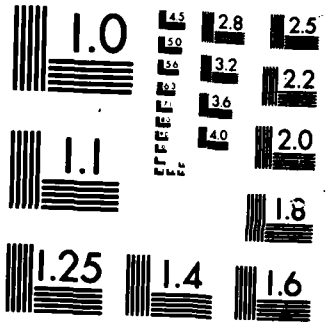

NRL Memorandum Report 5732

Direct Numerical Simulation of Axisymmetric Jets

F. F. GRINSTEIN,* ELAINE S. ORAN AND J. P. BORIS

Laboratory for Computational Physics

**Berkeley Research Associates, Inc.*
Springfield, VA 22151

March 25, 1986

NAVAL RESEARCH LABORATORY
Washington, D.C.

AD-A165536

SECURITY CLASSIFICATION OF THIS PAGE

REPORT DOCUMENTATION PAGE

1a REPORT SECURITY CLASSIFICATION UNCLASSIFIED	1b RESTRICTIVE MARKINGS
2a SECURITY CLASSIFICATION AUTHORITY	3 DISTRIBUTION / AVAILABILITY OF REPORT
2b DECLASSIFICATION / DOWNGRADING SCHEDULE	Approved for public release; distribution unlimited.
4 PERFORMING ORGANIZATION REPORT NUMBER(S) NRL Memorandum Report 5732	5 MONITORING ORGANIZATION REPORT NUMBER(S)
6a NAME OF PERFORMING ORGANIZATION Naval Research Laboratory 6b OFFICE SYMBOL (If applicable) Code 4040	7a NAME OF MONITORING ORGANIZATION
6c ADDRESS (City, State, and ZIP Code) Washington, DC 20375-5000	7b ADDRESS (City, State, and ZIP Code)
8a NAME OF FUNDING / SPONSORING ORGANIZATION Office of Naval Research 8b OFFICE SYMBOL (If applicable)	9 PROCUREMENT INSTRUMENT IDENTIFICATION NUMBER
8c ADDRESS (City, State, and ZIP Code) Arlington, VA 22217	10 SOURCE OF FUNDING NUMBERS PROGRAM ELEMENT NO: 61153N13 PROJECT NO: RR013-06-4F TASK NO: WORK UNIT ACCESSION NO: DN155-537

11 TITLE (Include Security Classification)
Direct Numerical Simulation of Axisymmetric Jets

12 PERSONAL AUTHOR(S)
Grinstein, F. F.,* Oran, Elaine S. and Boris, J. P.

13a TYPE OF REPORT	13b TIME COVERED FROM ____ TO ____	14 DATE OF REPORT (Year, Month, Day)	15 PAGE COUNT
Interim		1986 March 25	17

16 SUPPLEMENTARY NOTATION
*Berkeley Research Associates, Inc., Springfield, VA 22151

17 COSATI CODES			18 SUBJECT TERMS (Continue on reverse if necessary and identify by block number)
FIELD	GROUP	SUB-GROUP	Numerical simulations; Coherent structures; Kelvin-Helmholtz; Free shear flows

19 ABSTRACT (Continue on reverse if necessary and identify by block number)

We present results from numerical simulations of the evolution of the Kelvin-Helmholtz instability for an unforced, subsonic, compressible axisymmetric, spatially-evolving shear layer. In addition, we study the effect of small, random pressure fluctuations at the nozzle orifice on the growth of the mixing layers. These fluctuations model inflow perturbations in experimental flows arising from turbulence and boundary layers in the nozzle. The finite-difference numerical model used to perform the simulations solves the two-dimensional time-dependent conservation equations for an ideal fluid using the Flux-Corrected Transport algorithm and timestep-splitting techniques. No subgrid turbulence model has been included. In the absence of perturbations, the calculations indicate that the large scale development of the unforced jet shear layer has an underlying degree of organization. This is the result of a feedback mechanism in which the shear layer ahead of the nozzle edge is modulated by the far field induced by the mergings downstream, near the end of the potential core of the jet. The studies with random high frequency perturbations on the inflow velocity show that they effectively tend to break the temporal correlations between the structures.

20 DISTRIBUTION / AVAILABILITY OF ABSTRACT ☒ UNCLASSIFIED/UNLIMITED ☐ SAME AS RPT ☐ DTIC USERS	21 ABSTRACT SECURITY CLASSIFICATION UNCLASSIFIED
22a NAME OF RESPONSIBLE INDIVIDUAL Elaine S. Oran	22b TELEPHONE (Include Area Code) (202) 767-2960 22c OFFICE SYMBOL Code 4040

DD FORM 1473, 84 MAR 83 APR edition may be used until exhausted
All other editions are obsolete

SECURITY CLASSIFICATION OF THIS PAGE

CONTENTS

DIRECT NUMERICAL SIMULATION OF AXISYMMETRIC JETS

Introduction

Experimental investigations in the last decade have shown that large spanwise coherent structures dominate the entrainment and mixing processes in shear layers [1]. Recently, it has become possible to study these structures by direct numerical simulation of their large scale features. These simulations are an important alternative and supplementary tool in the basic research of the properties of fluid flow transitioning to turbulence. Since a simulation can calculate values for all the primary flow field properties as a function of time, statistical information can be obtained about the system through spatial and temporal averages. In addition, parameters of the flow can be easily varied. While the experimental conditions may not be fully controllable in the laboratory, the simulation conditions are.

Numerical studies of coherent structures have used spectral [2], vortex dynamics [3], and finite-difference [4–6] techniques. Numerical studies of the evolution of flows similar to those seen in the laboratory experiments have considered both two-dimensional planar and axisymmetric shear layers. Previous finite-difference calculations have modeled either temporally-developing mixing layers [4], where it is assumed that the relevant vortex dynamics takes place in relatively compact space regions, or spatially developing layers [5–7], which represent the more realistic situations occurring in the laboratory.

In previous work we have performed finite-difference, compressible, spatially-developing simulations of planar shear flows, with the objective of investigating asymmetries in mixing [6] and the basic mechanisms involved in the reinitiation of the instabilities [7]. Here we describe finite-difference calculations of the evolution of the Kelvin-Helmholtz instability for a spatially-evolving compressible axisymmetric jet emerging into a quiescent background. The instabilities sustain themselves through a feedback mechanism in the flow. The evolution and merging of the downstream structures affect the inflowing material upstream, thus triggering the growth and shedding of new vortices [7]. In addition, we study the effect of small, random pressure fluctuations at the nozzle orifice on the growth of the mixing layer. These fluctuations model inflow perturbations in experimental flows arising from turbulence and boundary layers in the nozzle.

Manuscript approved December 10, 1985.

The Numerical Model

The numerical model used to perform the simulations solves the two-dimensional time-dependent conservation equations for mass, momentum and energy for an ideal gas

$$\frac{\partial \rho}{\partial t} = -\nabla \cdot \rho \mathbf{V}, \tag{1}$$

$$\frac{\partial (\rho \mathbf{V})}{\partial t} = -\nabla \cdot \rho \mathbf{V}\mathbf{V} - \nabla P, \tag{2}$$

$$\frac{\partial \epsilon}{\partial t} = -\nabla \cdot \epsilon \mathbf{V} - \nabla \cdot P\mathbf{V}, \tag{3}$$

where $\epsilon = P/(\gamma - 1) + (1/2)\rho V^2$, is the internal energy, and $\mathbf{V}$, P, ρ, and γ, are the velocity, pressure, mass density, and the ratio of specific heats. The equations are solved using the Flux-Corrected Transport (FCT) algorithm [8] and timestep-splitting techniques. FCT is an explicit, fourth-order, finite-difference algorithm, which ensures that all conserved quantities remain monotonic and positive. FCT modifies the linear properties of a high order algorithm by adding diffusion during convective transport to prevent dispersive ripples from arising. The added diffusion is subtracted out appropriately where not needed in an anti-diffusion phase of the integration cycle to maintain high order accuracy. With this approach, no artificial viscosity is required to stabilize the algorithm.

The model uses inflow and outflow boundary conditions which have been developed and tested for these types of multidimensional FCT calculations [6,9]. The conditions ensure the proper behavior of the fluid near the boundaries. The inflow boundary conditions specify the inflow density and velocity, and use a zero slope condition on the pressure at the inflow boundary to define the energy at the guard cells:

$$\rho_g = \rho_{inflow}, \tag{4a}$$

$$v_g = v_{inflow}, \tag{4b}$$

$$P_g = P_1, \tag{4c}$$

where P_1 is the pressure at the first (inflow) cell. This allows pressure differences between the jet and the surrounding fluid to generate transverse flows. In addition, a short inflow plenum is modelled by including a portion of the nozzle within the computational domain. The outflow boundary conditions define the density and velocity at the guard cells by means of extrapolations from the last two cells:

$$\rho_g = \rho_n, \tag{5a}$$

$$v_g = 2v_n - v_{n-1}. \tag{5b}$$

The guard cell pressure, in turn, is defined by interpolating between the boundary pressure value and ambient pressure (assumed at infinite distance from the trailing edge of the nozzle):

$$P_g = P_n + \frac{(Y_g - Y_n)}{(Y_g - Y_j)}(P_{amb} - P_n), \tag{5c}$$

where Y is either the radial or axial coordinate, and the subscript j refers to the trailing edge of the nozzle. In this way, the outflow boundary conditions impose a slow relaxation of the pressure towards the known ambient value. These boundary conditions allow feedback to occur between the downstream vortices and the inflowing material. This physically realistic approach avoids the need to constantly drive the instability, allowing for it to evolve naturally in the calculation. No subgrid turbulence model has been included. The simulations are expected to be adequate in describing large scale features of gas phase flow for large Reynolds numbers.

The computational grid was set up initially and held fixed in time. The timesteps were chosen to satisfy the Courant condition. The basic finite-difference grid used 120 cells in the cross-stream (radial) direction and 220 in the streamwise (axial) direction, with the mesh spacings varying in the ranges $0.05 \leq \Delta Z \leq 0.52$ cm and $0.02 \leq \Delta R \leq 0.067$ cm. Figure 1 shows a schematic diagram of the grid. The cells are closely spaced in the radial (R) direction across the shear layer, where the large structures form, and they become farther apart as the distance from the shear layer increases for $R > R_o$. The cell separations in the streamwise direction (Z) also increase in size as we move downstream and upstream from the trailing edge of the nozzle, located at $R = R_o = 0.9$ cm, $Z = Z_o \approx 1.67$ cm. This takes advantage of the fact that the structures merge and grow downstream, so that fewer cells are necessary to keep the same relative resolution as obtained near the nozzle. Convergence of the results was verified by checking their consistency with results obtained on grids with 440×120 and 220×240 computational cells, which doubled the resolution in the axial and radial directions, respectively, relative to the 220×120 grid.

The Unforced Axisymmetric Jet

The system studied is a high speed jet containing a mixture of molecular hydrogen and nitrogen emerging into a quiescent background mixture of molecular oxygen and nitrogen, with a jet to background density ratio of 0.67. The system was initialized with a step function axial velocity profile at a uniform temperature (298 K) and pressure (1 atm). The jet was subsonic, with Mach number 0.57, and corresponding velocity 2.0×10^4 cm/s. Figure 2 is a schematic diagram of the flow configuration. The perturbation, which initiated the instabilities and occurred only at the very beginning of the calculation, is a very small cross-stream pressure gradient generating vorticity at the shear layer just ahead of the nozzle edge. This disturbance moves downstream as the integration proceeds, generating the transverse flows which trigger the Kelvin-Helmholtz instability. Previously, initial sinusoidal perturbations along the shear interface were considered [9]. The current approach to initiating the instability was used in the simulation of planar shear flows [6,7], and is closely analogous to using a delta function perturbation at the center in an idealized periodic simulation involving two equal and opposite streams.

Typical features of the flow at the early stages are shown in the sequence of isovorticity contours in Fig. 3. Vortex rings develop because of the non-linear growth of the instability. This occurs at an essentially fixed distance from the nozzle edge, somewhat less than one diameter $D = 2R_o$, at $z = (Z - Z_o)/D \approx 0.4$. The newly formed structures move along the interface, interact with each other and thereby spread the vorticity

until the center, potential core region disappears, at approximately $z = 3$. The structures are displaced vertically by a low-frequency modulation of the shear layer. When appropriately phased with the structures, the modulation tends to favor the merging of three structures in half of the modulation cycle, where they will coalesce into larger structures. Since the jet is unforced, the low-frequency modulation can only be due to the pressure field induced by the larger structures downstream, as they pass near the end of the potential core of the jet. As the effect of the downstream events on the inflowing fluid becomes important, there is an interaction between the basic instability mechanism at the shear layer and the feedback mechanism. The flow pattern becomes subsequently different from that at the initial stages in the flow development, which is dominated by the shear layer instability. A striking feature, on the last panel of Fig. 3, is the spatial coherence between the structures. This is characteristic of the feedback phenomena between the downstream events and the inflowing fluid in jets [10]. The distance between the second and the third merging locations increases, relative to the distance between the second and the first mergings, by a factor of the order of 2 - 3, in good agreement with the results of jet experiments with low-level acoustical excitation [12].

Frames at much later times in the development of the flow can be seen in Fig. 4. A noticeable feature of this sequence of frames is a regular repeating spatial pattern in the evolution of the flow. We have performed a spectral analysis of the axial (streamwise) velocity fluctuations, based on the results of the calculations for these later times. In the sequence of panels in Fig. 5, we show the results of the analysis at various relevant axial locations on the center of the shear layer ($R = R_o$), and in terms of the normalized (Strouhal) frequency $St = 2\pi f \theta_o / v_o$, where θ_o and v_o are the initial momentum thickness of the shear layer and the jet velocity, respectively. The latter thickness was taken to be effectively defined by $\theta_o = \Delta R = 0.02$ cm, where ΔR is the size of a radial cell in the region of the shear layer (within which the step of the initial velocity profile is defined).

Figure 5a, at $z = 0.4$, corresponding to a location near the nozzle exit, shows peaks located at the frequencies $St_o \approx 0.100$, $St_1 \approx 0.050$, $St_2 \approx 0.025$, $St_+ \approx 0.125$, and $St_- \approx 0.075$. Here, St_o can be associated with the shear layer instability frequency, in good quantitative agreement with the predictions of linear inviscid instability theory [13]. In addition, the modulation of the initial shear layer with $St_1 \approx St_o/2$ and $St_2 \approx St_o/4$ is associated with the first and second subharmonic, while $St_\pm \approx (St_o \pm St_2)$ result from the non-linear interaction between the shear layer instability and the feedback process. Moreover, we note that the low frequency peak is located at non-dimensional frequency $St_{jet} = fD/v_o \approx 0.36$. This is within the range $0.2 \leq St_{jet} \leq 0.5$, where the frequency of the preferred jet mode (characteristic of the largest scales on an unforced subsonic jet) is known to lie [12]. As we move downstream, the amplitudes for the high frequencies tend to diminish, as can be expected. In particular, Figs. 5b,c indicate locations of the beginning and concluding stages, respectively, of a first merging (associated with St_1). Similarly, Figs. 5d and 5e correspond to locations where second (associated with St_2) and third (associated with $St_3 \approx St_o/8$) mergings take place.

The detailed flow visualization through the sequence of panels in Fig. 6 allows to determine the approximate pairing locations, as defined by the locations where the vertical alignment of the vortices takes place. In this way the locations of the second and third pairings can be estimated from panels c) and d), respectively, at $Z \approx 4.8$ cm, and $Z \approx 9.7$ cm. The beginning of the first pairing can be also observed in panel d), at $Z \approx 3.3$ cm, where the vortices are seen in the process of rolling around each other. There is a close agreement between these merging locations obtained by direct flow visualization, and the results of the spectral analysis above. Note, in particular, that the third merging actually occurs downstream of the end of the potential core of the jet. Because of this, the effect of this merging on the shear layer just ahead of the trailing edge of the nozzle is negligible, as indicated by the spectral distribution in Fig. 5a. This is evidence of the role of the jet diameter, and hence of the location of the end of the potential core, in the selection of the dominant low frequency mode of the jet.

Effect of Random Inflow Perturbations

We have also simulated the effects of high frequency random perturbations in the inflowing jet stream. Such fluctuations are typically present in the experimental conditions in the laboratory, and are due to turbulence and boundary layers in the nozzle. In the calculations this is done by replacing the streamwise velocity U at the inflow (i.e., for $Z = 0.0$ cm, $R \leq R_o$) with $U(1+p)$, where $p = p(R,t)$ is the perturbating term. This term is defined by a sine Fourier series in the variable R, with R_o the largest wavelength:

$$p(R,t) = \frac{1}{m} \sum_{m=1}^{M} p_m^o \delta_m(t) sin(\frac{2\pi m R}{R_o} + \phi_m), \qquad (6)$$

where $\delta_m(t)$ is a time-dependent amplitude defined by

$$\delta_m(t) = \frac{2(t - t_{om})}{\delta t_m}, \quad \text{if } t_{om} \leq t \leq \frac{(t_{om} + \delta t_m)}{2},$$

$$\delta_m(t) = \frac{2(t_{om} - t)}{\delta t_m} + 2, \quad \text{if } \frac{(t_{om} + \delta t_m)}{2} \leq t \leq t_{om} + \delta t_m,$$

and by

$$\delta_m(t) = 0,$$

otherwise. In this way, each added perturbation term varies between 0.0 and a maximum value of no more than a fraction p_m^o/m of the inflow jet velocity. The duration δt_m, and maximum value p_m^o of the amplitude, as well as the intrinsic phases $\phi_m (0 \leq \phi_m \leq 2\pi)$ of the terms in the Fourier series are randomly generated numbers.

A calculation was performed which restarted the program at time $t = 2.52$ ms of the previous unperturbed calculation, but now including inflow fluctuations. Here, the series in eq. (6) was truncated to its first four terms (M=4), including only fluctuations of wavelength $R_o, R_o/2, R_o/3$, and $R_o/4$, with durations δ_m in the range of $5 - 12.5$ μs (20 – 50 time steps). Due to the changes in the frequency content of the velocity

field, the previous regularity in the flow pattern was lost in spite of the relatively small amplitude of the fluctuations. This can be seen by comparison of the spectral distributions obtained in this case with those for the unperturbed case discussed above. We compare Figs. 7a-c, for mean perturbation levels of 0.1, 1 and 5 %, respectively, with Fig. 5a. This indicates that the peaks become broader, while new high frequency peaks are now present. As the fluctuation level increases, the calculated spectral distribution begins to look like the distributions obtained in the analysis of near field pressure fluctuations in experiments with non-excited-jets [12]. The experimentally obtained distributions consist of a broad peak tilted towards the low frequency side, and centered on $St_{jet} \approx 0.37$, in agreement with the value of St_{jet} found in the present numerical simulations.

Summary and Conclusions

We have presented results from numerical simulations of the evolution of the Kelvin-Helmholtz instability for a subsonic, compressible, axisymmetric, spatially-evolving shear layer. In the absence of boundary layers and small-scale inflow turbulence, the calculations indicate that the large-scale development of the unforced jet shear layer has an underlying degree of organization. This is the result of a feedback mechanism in which the shear layer ahead of the nozzle edge is modulated by the far field induced by the mergings downstream, near the end of the potential core of the jet. This is in agreement with the experimental observations [12].

The dominant frequencies in the unforced flow depend on the two length-scales of the jet, namely, the initial shear layer thickness and the jet diameter. These scales are associated with the two basic mechanisms in the jet, the jet shear layer instability and the jet column instability, which determine the high and low frequency natural modes of the jet, respectively. The spectral analysis of the axial velocity fluctuations at the center of the shear layer, just ahead of the nozzle edge, shows a sequence of peaks separated by a regular interval approximately equal to $St_o/4$. These peaks correspond to the subharmonics of the jet shear layer instability frequency St_o and to the non-linear interactions between them. The non-dimensional frequency of the preferred jet mode, $St_{jet} = (f_o/4)D/v_o \approx 0.36$, is in good agreement with the experimental values for subsonic jets. Moreover, the value for St_o was consistent with the predictions of linear inviscid instability theory. In addition, the distribution of the merging locations was in qualitative agreement with that observed in jet-experiments with low-level forcing.

The studies with random high frequency perturbations on the inflow velocity show that such perturbations tend to break the organized jet shear layer, and hence the temporal coherence between the structures. By generating more incoherent mergings the fluctuations tend to destroy the regularity of the idealized, unforced two-dimensional case.

Acknowledgments

We would like to acknowledge useful discussions with Dr. K. Kailasanath. This work was sponsored by the Mechanics Division of the Office of Naval Research and by the Naval Research Laboratory.

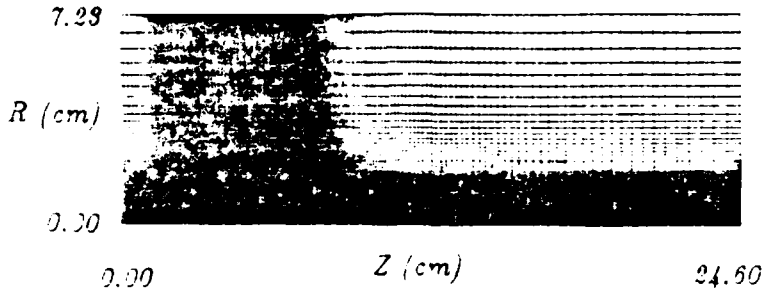

Fig. 1: Schematic diagram of the 220 × 120 computational grid.

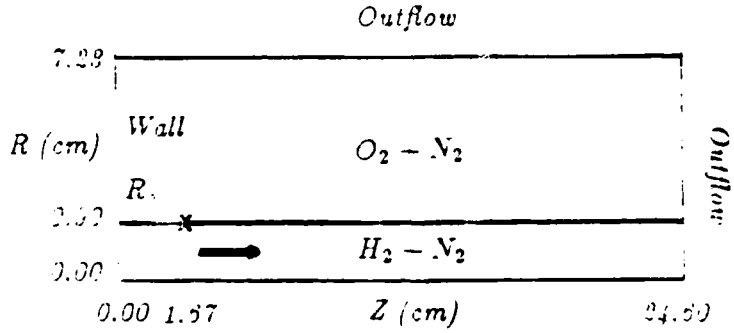

Fig. 2: Flow configuration for the axisymmetric jet simulation. The 'x' indicates the location of the trailing edge of the nozzle.

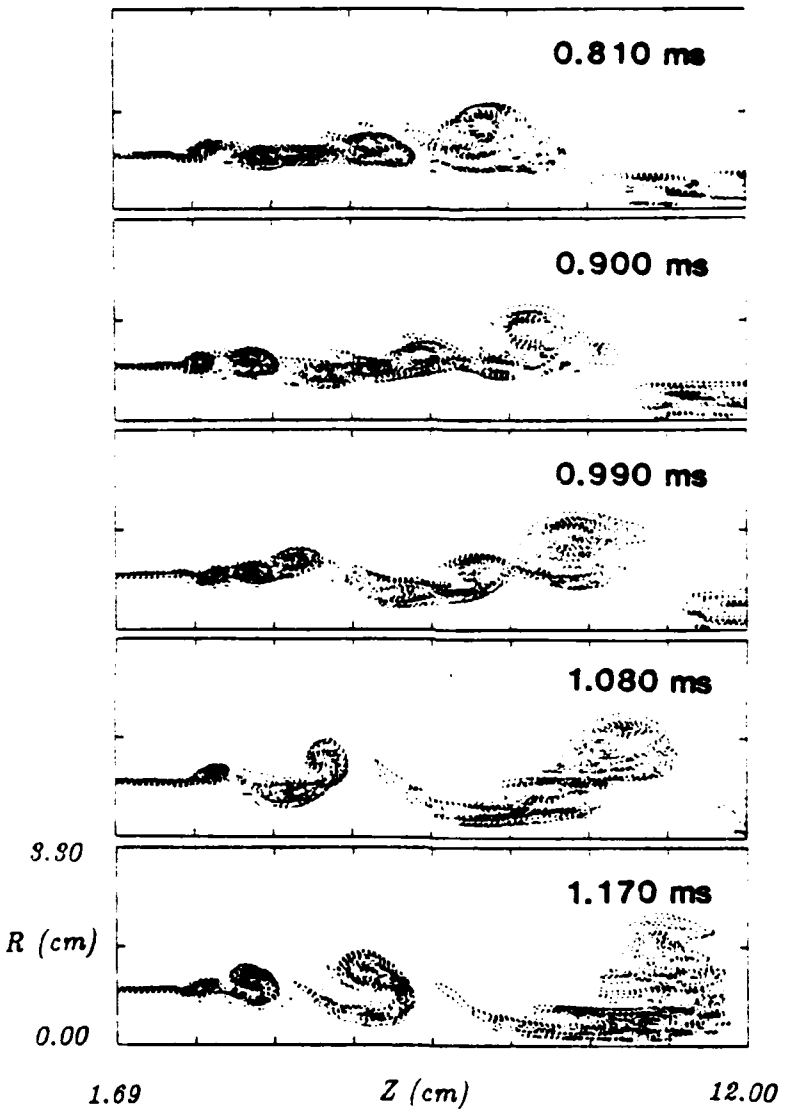

Fig. 3: Initial stages in the flow development.

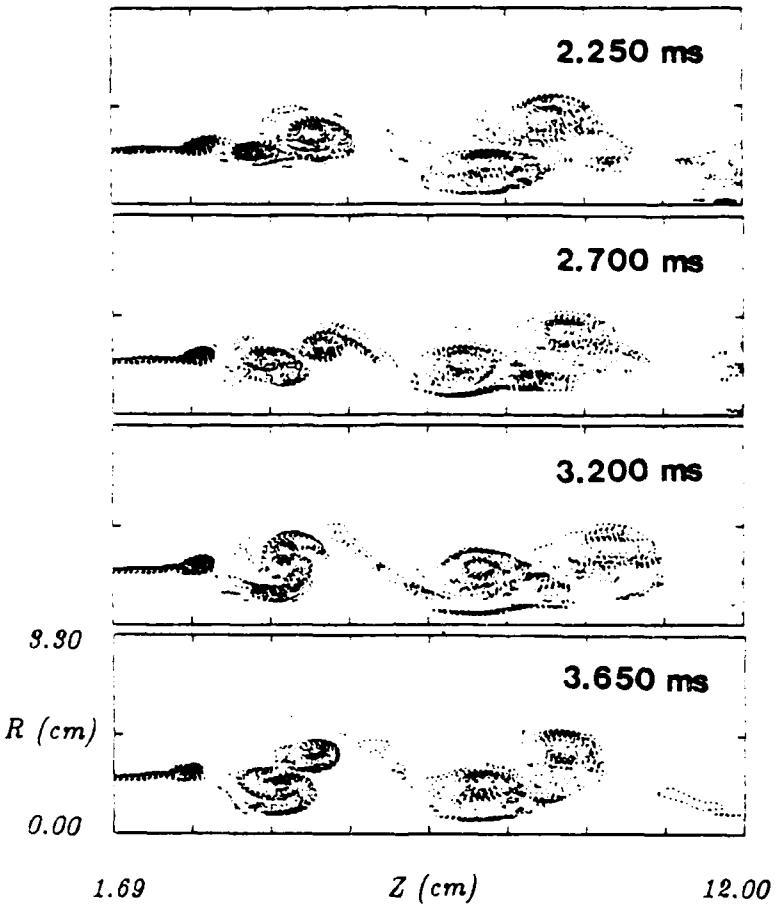

Fig. 4: Regularity and spatial coherence of the flow development for the unforced jet.

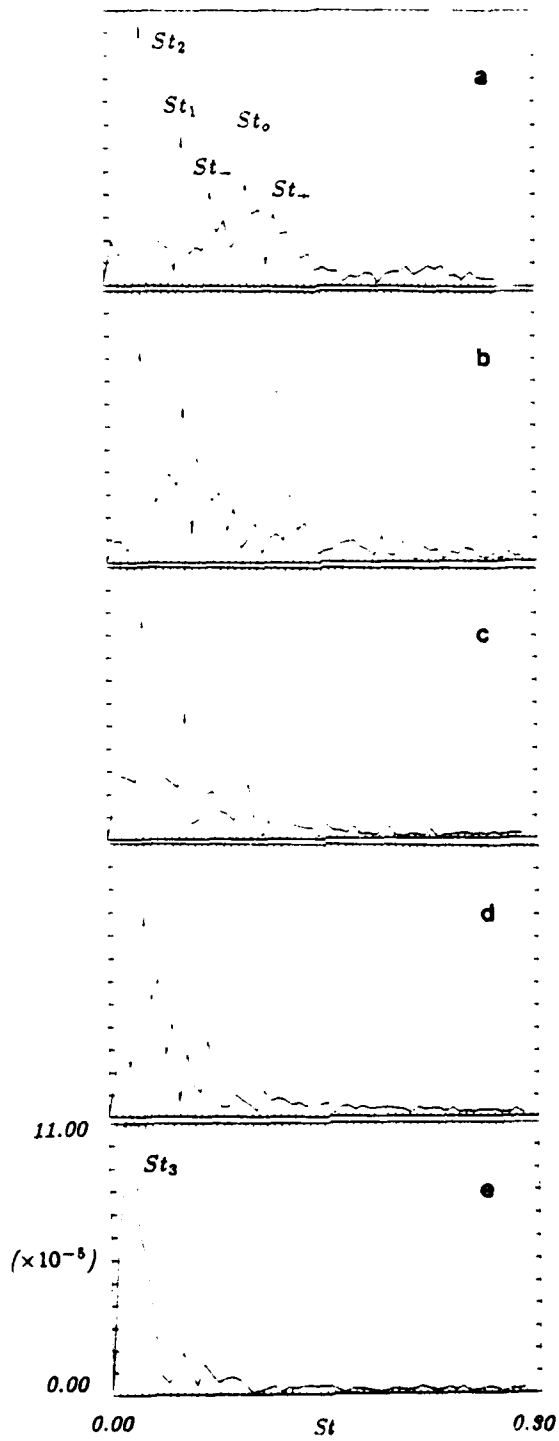

Fig. 5: Spectral amplitude at $R = D/2$, and various axial locations, as a function of Strouhal frequency St. a) $Z = 2.39$ cm ($z = 0.40$); b) $Z = 2.94$ cm ($z = 0.71$); c) $Z = 3.54$ cm ($z = 1.04$); d) $Z = 5.24$ cm ($z = 1.98$); e) $Z = 9.44$ cm ($z = 4.32$).

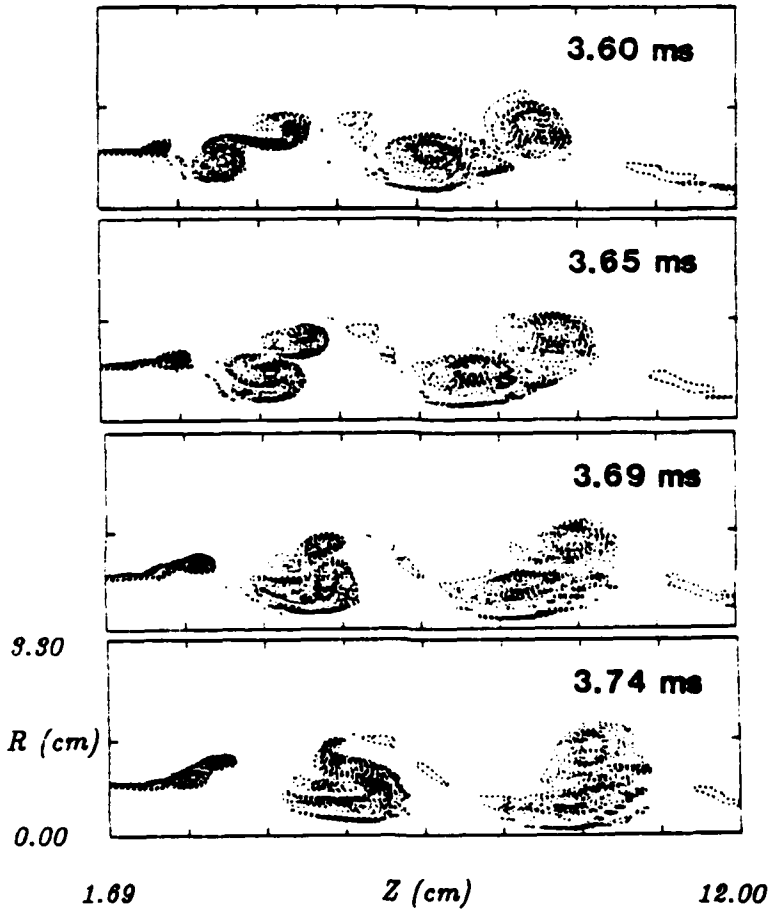

Fig. 6: Flow visualization showing detailed vortex mergings.

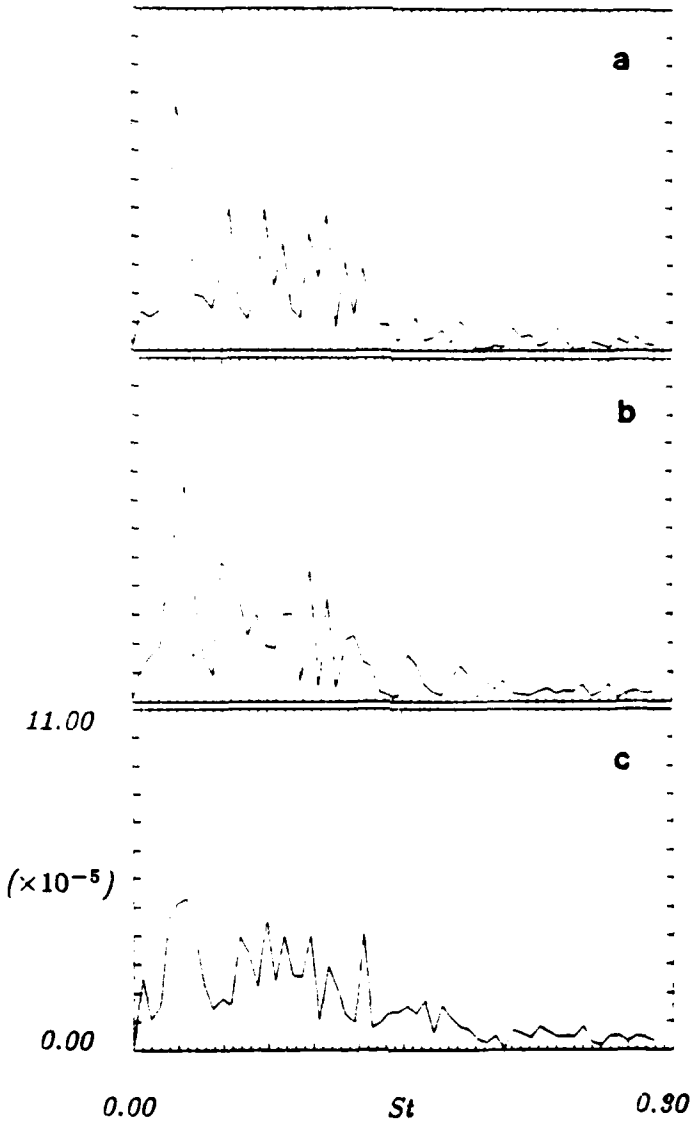

Fig. 7: Spectral amplitude at $R = D/2$ and $Z = 2.39$ cm $(z = 0.40)$, as a function of the Strouhal frequency, for the randomly perturbed jet with, a) 0.1 %, b) 1 %, and c) 5 % fluctuation levels.

References

[1] Winant, C. D. and Browand, F. K., *J. Fluid Mech.* **63**, 237 (1974). Brown, G. and Roshko, A., *J. Fluid. Mech.* **64**, 775 (1974). Browand, F.K. and Ho, C. M., *Journal de Mécanique Théorique et Apliquée*, Numéro spécial, pp. 99-120 (1983), and references therein.

[2] Leonard, A., *J. Comp. Phys.* **37**, 289 (1980).

[3] Riley, J. J. and Metcalfe, R. W., in *Proc. of the Seventh Int. Conf. on Num. Meth. in Fluid Mech.*, ed. by W. C. Reynolds and R. W. MacCormack, Springer, New York, 1981, p. 279.

[4] Corcos, G. M. and Sherman, F. S., *J. Fluid Mech.* **139**, 29 (1984).

[5] Davis, R. W. and Moore, E. F., *Phys. Fluids* **28**, 1626 (1985).

[6] Grinstein, F. F., Oran, E. S. and Boris, J. P., "Direct Simulation of Asymmetric Mixing in Planar Shear Flows", to appear in *J. Fluid Mech* (1986); see also NRL Memorandum Report 5621 (1985), Naval Research Laboratory, Washington, DC.

[7] Grinstein, F. F., Oran, E. S. and Boris, J. P., "Kelvin-Helmholtz Instability in unforced Spatially-Developing Mixing Layers", to be submitted to *J. Fluid Mech* (1985).

[8] Boris, J. P. and Book, D., in *Meth. in Comp. Phys.*, Vol. 16, Ch. 11, Academic Press, 1976; see also Boris, J. P., NRL Memorandum Report 327 (1976), Naval Research Laboratory, Washington, DC.

[9] Boris, J. P., Oran, E. S., Gardner, J. H., Grinstein, F. F. and Oswald C. E., in *Ninth Int. Conf. on Num. Meth. in Fluid. Mech.*, ed. by Soubbaramayer and J. P.Boujot, Springer, NY, 1985, pp. 98-102.

[10] Laufer, J., in *Transition and Turbulence*, ed. by R.E. Meyer, pp. 63-76, Academic Press, N.Y. (1981).

[11] Laufer, J. and Monkewitz, P.A., *AIAA paper* 80-0962, Hartford.

[12] Kibens, V., *AIAA J.* **18**, 434 (1980).

[13] Michalke, A., "Instability of compressible circular free jet with consideration of the influence of the jet boundary layer thickness", *NASA Tech. Memo* 75190 (1977); Michalke, A. and Hermann, G., *J. Fluid Mech.* **114**, 343 (1982).

END
FILMED
4-86
DTIC